Astronomical and Astrophysical Transactions (*AApTr*), 2012, Vol. 27, Issue 2, pp. 197–210,
ISSN 1055-6796, Photocopying permitted by license only, ©Cambridge Scientific Publishers

Diffusion in barred-spiral galaxies

Maura Brunetti[1*], Cristina Chiappini[2], Daniel Pfenniger[1]

[1] *Geneva Observatory, University of Geneva, CH-1290 Sauverny, Switzerland*
[2] *Leibniz-Institut für Astrophysik Potsdam (AIP), An der Sternwarte 16 D-14482, Potsdam, Germany*

Received 1 February, 2012

We characterize the radial migration of stars in the disk plane by calculating the diffusion coefficient and the diffusion time-scale for a bulge-disk N-body self-consistent system with a marginally-stable Safronov–Toomre parameter $Q_{\rm T}$. We find that diffusion is not constant in time, but follows the evolution of the bar, and becomes maximum near the corotation region and in the external disk region, where asymmetric patterns develop.

Keywords: Galaxies: kinematics and dynamics; Galaxies: stellar content; Galaxies: spiral; Galaxy: disk

1 Introduction

The majority of local galaxies are barred-spiral galaxies, such as our Milky Way [1, 2] where the bar is the strongest non-axisymmetric pattern in the disk. The bar is generally coupled to other non-axisymmetric patterns such as spirals and warps if the disk is sufficiently cold [3]. The bar has a time-dependent activity, with a pattern speed which typically decreases in isolated galaxies. However, the system can be cooled again by adding dissipative infall of gas, or by forming stars on low-velocity dispersion orbits, with the net effect of restoring the amplitude of spiral waves and the strength of the bar, or even destroying it. In this way bars (and spiral waves) can be seen as recurrent patterns which can be rebuilt during their long history until the present configuration at redshift $z = 0$ [4].

Under the action of these non-axisymmetric patterns, stars move in the disk which gradually becomes hotter. Velocity dispersion of disk stars rises with age, as confirmed by observations in the Solar neighborhood (see [5] and references therein) and in external galaxies [6, 7]. The origin and the amount of disk heating are still open to debate.

First attempts to explain such a heating process in the disk of galaxies tried to model empirically the observed increase of the stellar velocity dispersion with age in the solar neighborhood. Wielen [8] suggested a diffusion mechanism in velocity space, which gives rise to typical relaxation times for young disk stars of the order of

*Corresponding author. Email: Maura.Brunetti@unige.ch

the period of revolution and to a deviation of stellar positions of 1.5 kpc in 200 Myr. The result was obtained without making detailed assumptions on the underlying local acceleration process responsible for the diffusion of stellar orbits. Global acceleration processes, such as the gravitational field of stationary density waves or of central bars with constant pattern speed, were ruled out since their contribution to the velocity dispersion of old stars was found to be negligible and concentrated in particular resonance regions [8, 9]. Different local accelerating mechanisms have been investigated so far in isolated galaxies, such as the gravitational encounters between stars and giant molecular clouds [10–12], secular heating produced by transient spiral arms [13–15] or the combination of the two processes [16, 17].

The radial excursion predicted by Wielen [8] is not sufficient to explain the weakness of the correlation between age and metallicity in the Solar neighborhood (see, for example, [18]). In order to explain both the large scatter in the age-metallicity relationship and the evidence that even old disk stars today have nearly circular orbits, Sellwood & Binney [19] have suggested a new mechanism based on the resonant scattering of stars under the effect of transient spiral waves. In this process, a star initially on a nearly circular orbit resonates with a rotating wave and changes its angular momentum. If the duration of the peak amplitude of the perturbing potential is less than the period of the 'horseshoe' orbits, i.e. orbits of particles trapped at the corotation radius of the spiral wave, the star can escape from the potential well without changing its eccentricity. The net effect of this scattering mechanism is that stars migrate radially without heating the disk. In other words, the overall distribution of angular momentum is preserved, except near the corotation region of the transient spiral wave, where stars can have large changes of their angular momenta.

The mechanisms driving radial migration and heating are still hotly debated. Minchev et al. [20, 21] propose a mixing mechanism where resonances between the bar and the spiral arms can act much more efficiently than transient spiral structures, dramatically reducing the predicted mixing timescales.

Most of the observational signatures of radial mixing reported in the literature [22–24] point to stars coming from a region next to the bulge/bar intersection. Radial migration of the stars in the disk have been suggested by Haywood [25], who estimated upper values for the migration rate from 1.5 to 3.7 kpc/Gyr, which agree with the values estimated in [26] for the radial wandering due to the scattering mechanism assumed by Sellwood and Binney [19]. High resolution cosmological simulations [27] confirm that such scattering mechanism determines a significant migration in the stellar disk. However these simulations ignore the important effects of bars found by Minchev et al. [20, 21]. Radial migration of stars (and gas) could have important implications for the interpretation of key observational constraints, such as the age-metallicity relationship or the metallicity gradients, since old stars that formed at small galactocentric radii from enriched gas or young metal-poor stars at large radii are enabled to appear in a Solar-neighborhood sample. Due to the lack of detailed information on the process driving radial mixing, models of the Galactic chemical evolution have evaluated past history of the solar neighborhood and the formation and evolution of the abundance gradients assuming that the Galaxy can be divided into concentric cylindrical annuli, which evolve independently [28–32]. Recently, Schoenrich and Binney [33] explored the consequences of mass exchanges between annuli by taking into account the effect of resonant scattering of stars described before. This

approach appears to be successful to replicate many properties of the thick disk in the Solar neighborhood without requiring any merger or tidal event [34]. However, again in this case, the strong mixing mechanisms driven by bar resonances were not taken into account, casting thus doubts on some of their conclusions.

In order to include the effect of radial migration in chemical evolution models and to gain a global (chemical + kinematical) understanding of the processes at play in the galactic disks, many dynamical aspects need to be further investigated and in particular the role of the bar, that is the main non-axisymmetric component in disk galaxies. This is what we start to do in the present paper. In particular, we consider a marginally-stable disk which develops a central bar and spiral arms with the aim of quantitatively estimating the time and length scales of star diffusion in the radial direction. The final goal is to investigate how these characteristic scales evolve in time and how they depend on the activity of the bar. We present in detail the methods used for calculating the diffusion coefficient and time-scale. We apply these methods to models which include the halo component and disks with different degree of stability in [35].

The paper is organised as follows. In Section 2 we describe the simulation and the relevant parameters. In Section 3 we solve the diffusion equation in axisymmetric systems, we define the diffusion coefficient, the diffusion time-scale and the diffusion length-scale, and we describe how we estimate these quantities from the simulation results. In Section 4 we present our results and in Section 5 we summarise our findings.

2 N-body simulation

We have run self-consistent N-body simulations starting from a bar-unstable axisymmetric model. The initial configuration is marginally stable, i.e. the initial value of the Safronov–Toomre parameter $Q_{\rm T} = \sigma_{\rm r}\,\kappa/(3.36\,G\,\Sigma)$ is $Q_{\rm T} \sim 1$, where $\sigma_{\rm r}$ is the radial velocity dispersion of the disk component, G is the gravitational constant, Σ is the disk surface density, κ is the epicycle frequency defined by $\kappa^2 = Rd\Omega^2/dR + 4\Omega^2$, where Ω is the circular frequency related to the global gravitational potential $\Phi(R, z, t)$ in the disk plane $z = 0$ by $\Omega^2 = (1/R)\,\partial\Phi/\partial R$.

The initial mass distribution in our simulations corresponds to a superposition of a pair of axisymmetric Miyamoto–Nagai disks of mass $M_{\rm B}$, $M_{\rm D}$, horizontal scales $A_{\rm B} + B$, $A_{\rm D} + B$, and identical scale-height B,

$$\Phi_{\rm MN}(R, z) = \sum_{i={\rm B,D}} \frac{-GM_i}{\sqrt{R^2 + (A_i + \sqrt{B^2 + z^2})^2}}\,. \qquad (1)$$

The first component represents the bulge (B), while the second the disk (D) [36]. The parameters have been set to $A_{\rm B} = 0.07$ kpc, $A_{\rm D} = 1.5$ kpc, $B = 0.5$ kpc, $M_{\rm B}/M_{\rm D} = 3/17$. The initial particle positions and velocities are found by a pseudo-random draw following the density law corresponding to eq. (1), truncated to a spheroid of semi-axes $R = 30$ kpc, $z = 10$ kpc. The number of particles in the disk-bulge component is $N = 4 \cdot 10^6$ and the total mass is $M_{\rm BD} = 4.2 \cdot 10^{10}\ M_\odot$. We then solve for the first velocity moment equations (Jeans equations) to find an approximate local equilibrium. The resulting distribution is then relaxed for a couple of rotations

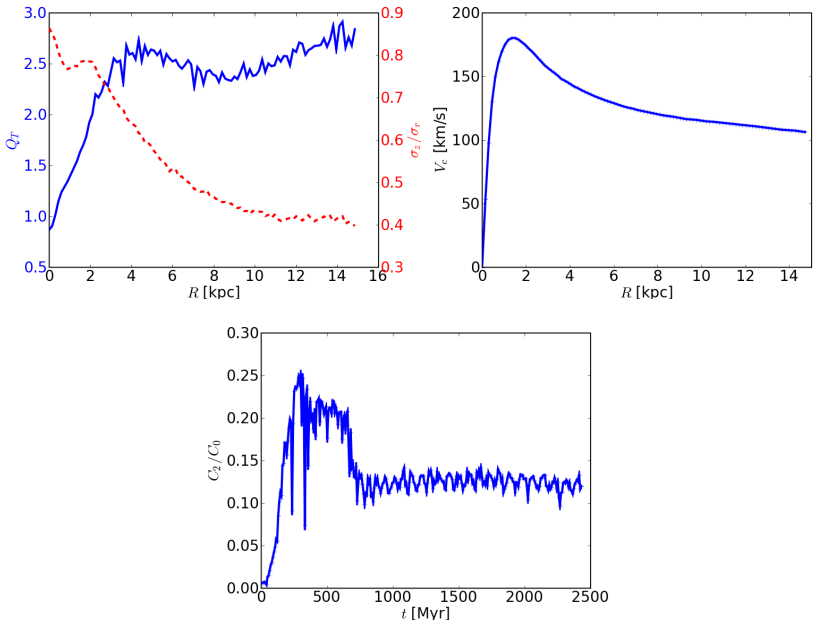


Figure 1 *Left*: Safronov–Toomre parameter (solid blue line) and Araki (σ_z/σ_r) parameter (dashed red line, labels on the right y-axis) at the final time. *Middle*: Rotation curve. *Right* Bar-strength time evolution.

until ripples spreading through the disk from the center disappeared. We used this as the initial condition for the N-body simulations, performed with the Gadget-2 code [37, 38].

The initial value of the radial and vertical velocity dispersions at two scale lengths from the center is $\sigma_r \sim \sigma_z \sim 20$ km/s. The disk is marginally stable and spiral waves develop with the main global effect of heating in the radial direction. The Safronov–Toomre and Araki parameters at the final time are shown in the left panel of Fig. 1, solid blue and dashed red lines, respectively. The rotation curve at the final time is shown in the middle panel of Fig. 1.

We classify stellar orbits into three dynamical categories [39, 36]: 1) the bar orbits and the disk orbits with the Jacobi integral $H = E - \Omega_p L_z$ smaller than the value at the Lagrangian points $L_{1,2}$, $H < H(L_{1,2})$, where E is the total energy and L_z is the z-component of the angular momentum. The particle separation in the bar or disk component can easily be done since the bar orbits have typically smaller values of L_z and E. 2) The hot orbits with $H \geq H(L_{1,2})$.

The bar pattern speed $\Omega_P \equiv d\theta/dt$, where θ is the azimuthal angle of the bar major axis (in the inertial frame) calculated by diagonalising the moment of inertia tensor of the bar particles, is 35 km s^{-1} kpc^{-1} at final times. We find that the pattern speed slowly decreases in time with a rate of a few km/s/kpc/Gyr in agreement with [40, 4]. The corresponding corotation radius R_c, obtained by the intersection of Ω_P with the circular frequency, $\Omega_P(t) = \Omega(R_c, t)$, increases in time (it ranges from 2 to 4 kpc in our simulation).

In order to understand the role played by the central bar on the distribution of stars in the disk, we follow the evolution of the bar strength in time. The amplitude C_m of the mode m in the density distribution is defined as

$$C_m = \left| \sum_j \exp(i\, m\theta_j) \right|, \tag{2}$$

where j labels the stars. The bar's strength is defined as the mode $C_{m=2}$ when the stars are restricted to the bar component. We normalise C_2 with respect to the number of stars in the bar component, C_0. This quantity is shown in the right panel of Fig. 1. Since we do not include the gas component in our model, we are not able to follow its evolution for times longer than a few Gyrs. After this typical time-scale, the bar amplitude saturates and the system reaches a quasi-steady state. Since the inclusion of the gas component necessarily requires the introduction of other less controlled parameters, such as the cooling rate of star formation, we prefer in this first study to limit the integration time by a couple of Gyrs.

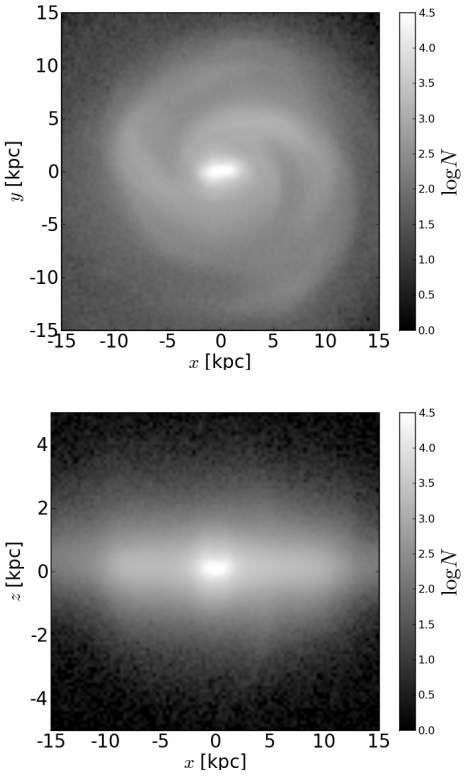


Figure 2 Density maps at $t \sim 550$ Myr. *Top*: face-on view. *Bottom*: edge-on view.

The face-on and edge-on views of the density distribution are shown in Fig. 2 at time $t \sim 550$ Myr, that is just after the moment when the bar's strength reaches its

maximum. Both bar and spiral arms develop, since the disk is sufficiently cold. In the external regions, the dominant mode is the pattern with $m = 1$.

3 Diffusion equation in axisymmetric systems

We model the diffusion along the radial direction in the galactic plane by introducing a distribution function $F(R, t)$ which satisfies the *spatial* diffusion equation in cylindrical coordinates

$$\partial_t F = \frac{D}{R}\,\partial_R(R\partial_R F)\,, \tag{3}$$

where D is the diffusion coefficient. The general solution of eq. (3) which is non-singular at $R = 0$ is given by

$$F(R,t) = \int_0^\infty A(s)\, e^{-Dts^2}\, J_0(sR)\, s\, ds\,, \tag{4}$$

where $J_0(x) = J_0(-x)$ is the Bessel function of the first kind. The function A can be determined by taking the Hankel transform of $F(R, 0)$

$$A(s) = \int_0^\infty F(R,0)\, J_0(sR)\, R\, dR\,. \tag{5}$$

Thus, by inserting eq. (5) into eq. (4) and assuming that the particles are initially localized at a certain radius R_0 at time $t_0 = 0$, $F(R, 0) = F_0 R_0 \delta(R - R_0)$, we obtain

$$F(R,t) = R_0^2 F_0 \int_0^\infty s\, e^{-Dts^2}\, J_0(sR)\, J_0(sR_0)\, ds\,. \tag{6}$$

The diffusion of this distribution can be expressed in terms of elementary and Bessel functions [41]. The time-evolution of an initial set of localized particles reads

$$F(R,t) = \frac{R_0^2 F_0}{2Dt} \exp\left(-\frac{R_0^2 + R^2}{4Dt}\right)\, I_0\left(\frac{RR_0}{2Dt}\right)\,, \tag{7}$$

where $I_0(x)$ is the modified Bessel function of the first kind, which is finite at the origin, $I_0(0) = 1$. In Fig. 3 two initial distributions with $D = 1$ and centered in $R_0 = 0.5$ and 2 (solid lines) evolve in time, as described by eq. (7) (dashed and dotted lines, respectively). At large radii, the distributions are essentially Gaussian, while at small radii they are strongly modified from the contributions of particles at the center of the cylinder. Equation (7) describes the distribution of the radial positions of stars in the disk at the initial time t_i which diffuse toward position R_0 at time t_0, such that $t_0 - t_i = \Delta t \leq T_{\rm D}$, where $T_{\rm D}$ is the diffusion time-scale or, equivalently, the distribution of stars which initially are in R_0 at t_0 and then diffuse toward R with $\Delta t \leq T_{\rm D}$.

For R which goes to zero, eq. (7) reduces to

$$F(0,t) = \frac{R_0^2 F_0}{2Dt}\, \exp\left[-R_0^2/(4Dt)\right]\,. \tag{8}$$

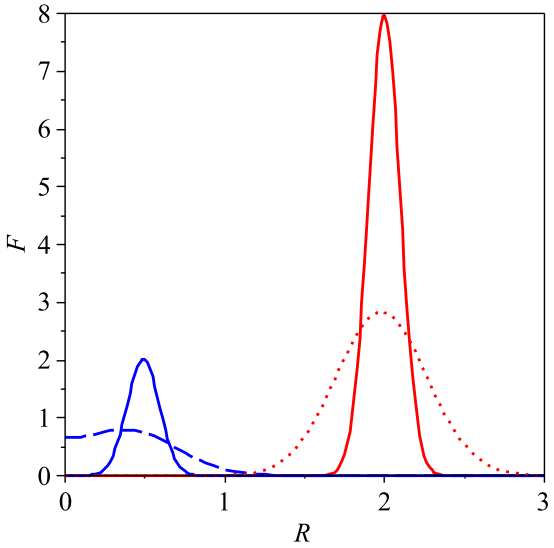


Figure 3 Two distributions with $D = 1$ and centered in $R_0 = 0.5$ and 2 (solid lines) evolve in time (dashed and dotted lines, respectively), as described by eq. (7).

For large values of the argument the modified Bessel function $I_0(x) \to (2\pi x)^{-1/2} \cdot \exp(x)$ and thus $F(R,t)$ reduces to

$$\lim_{R\to\infty} F(R,t) = \frac{R_0^{3/2} F_0}{\sqrt{4\pi D t R}} \exp\left(-\frac{(R-R_0)^2}{4Dt}\right) = \frac{R_0^{3/2} F_0}{\sqrt{R}} \mathcal{N}(\mu,\sigma) \qquad (9)$$

where $\mathcal{N}(\mu,\sigma)$ is the Gaussian distribution with mean value $\mu = \langle R \rangle = R_0$ and standard deviation $\sigma = \sqrt{2Dt}$.

As we will describe in the following subsection, the N-body simulation presented in Section 2 allows us to estimate the diffusion coefficient D and the diffusion time-scale $T_{\rm D} = |t_0 - t_i|$ in marginally stable disks.

3.1 Calculation of diffusion time-scale and diffusion coefficient

The diffusion coefficient D in eqs. (3)–(7) can be regarded as an instantaneous coefficient which depends on the position at which particles are initially localised and on the diffusion time. Modeling of stellar migration as a diffusion process is valid only for time intervals less than the diffusion time-scale, $\Delta t \leq T_{\rm D}$, and for time intervals larger than the typical chaotic time-scale. Thus, the first issue is to estimate this diffusion time-scale from the simulation results. In the top panel of Fig. 4, we show the radial dispersion $\langle \Delta R^2 \rangle$ of stars initially at (R_0, t_0) as a function of time, for different values of (R_0, t_0). At $t = t_0$ the radial dispersion is null since the particles are all localised at $R = R_0$. As time evolves, $\langle \Delta R^2 \rangle$ grows with a linear rate and then it saturates after a diffusion time-scale $T_{\rm D}$. The diffusion time scale turns out to be of the order of the rotation period, $T_{\rm D} \sim T_{\rm rot} = 2\pi/\Omega(R,t)$.

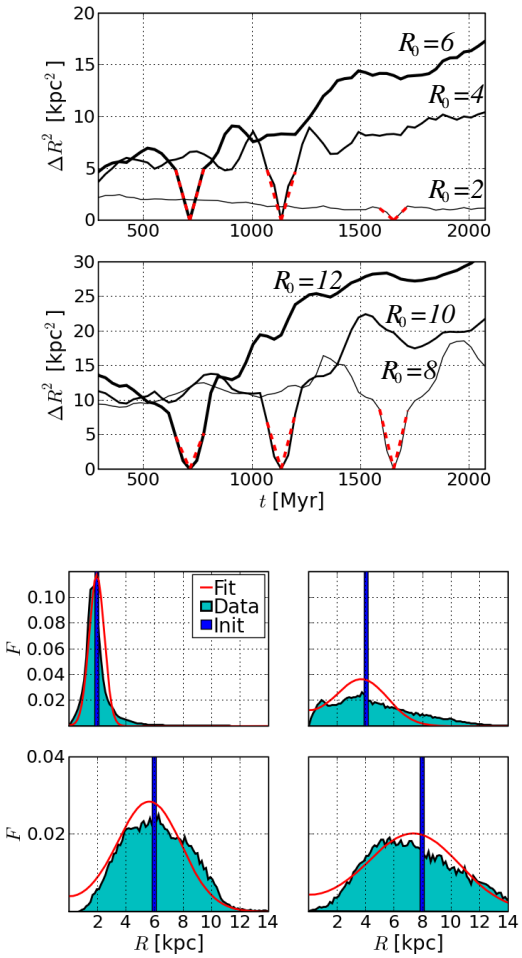


Figure 4 *Top:* radial dispersion of particles initially at (R_0, t_0), for $R_0 = 2, 4, \ldots, 12$ kpc and $t_0 = 700, 1150, 1650$ Myr, as a function of time. The growth rates in the vicinity of the initial time t_0 give a first estimate of the diffusion coefficient from the relation $\langle \Delta R \rangle^2 = \sigma^2 = 2Dt$ (dashed red lines). *Bottom*: distribution of particles at radius $R_0 = 2, 4, 6, 8$ kpc and different initial times t_0 (dark blue), distribution of the same particles at time t, such that $t - t_0 < T_{\rm D}$ (light blue) and fit calculated by the nonlinear least-squares method (red line).

From the relation $\langle \Delta R^2 \rangle = \sigma^2 = 2Dt$, we calculate a first estimate of the diffusion coefficient D as the growth rates in the vicinity of the initial time t_0 (red dashed lines in the top panel of Fig. 4) and we use these values as initial guess of the nonlinear least-square method, which minimizes the difference between the numerical results and the general solution of the diffusion equation described by eq. (7) for times less than $T_{\rm D}$. The maximum relative error on the estimated parameter D is $\Delta D/D \sim 0.06$ near the central region. The fitting function that we obtain by this procedure reproduces reasonably well the overall distribution of particles at times $t > t_0$ (or $t < t_0$), with $\Delta t = |t - t_0| < T_{\rm D}$, as can be seen in the bottom panel of Fig. 4.

4 Results

The methods described in the previous section allowed us to calculate the diffusion coefficient $D(R,t)$, which is shown in the contour map in the top panel of Fig. 5. The bar's corotation radius is also shown as a dashed white line. We can see that the diffusion coefficient is not constant in time nor in radius. If the disk is not too hot, D has the largest values $D \sim 0.12$ kpc^2 Myr^{-1} near the corotation radius of the bar (which increases in time in our simulation), where the density is strongly perturbed by an $m = 2$ pattern created by the bar and the transient spiral arms, and in the external regions $R > 8$ kpc, where the density is modulated by an $m = 1$ pattern. The stars respond collectively to these modulations and the process of migration corresponds to a diffusion in an axisymmetric system.

From D we can estimate the radial dispersion σ in a rotation period (which is of the order of the diffusion time-scale), $\sigma = \sqrt{2\,D\,T_{\rm rot}}$. If the disk is sufficiently cold, the radial dispersion is high near the corotation region of the bar, where it can recurrently assume values of the order of $\sigma \sim 6$ kpc. At an intermediate radius, such as $R = 6$ kpc, the radial dispersion is of the order of $\sigma \sim 3$ kpc and it increases in the external less dense regions where the pattern $m = 1$ dominates. In this external region, the radial migration is very high and the number of stars which stay in a local

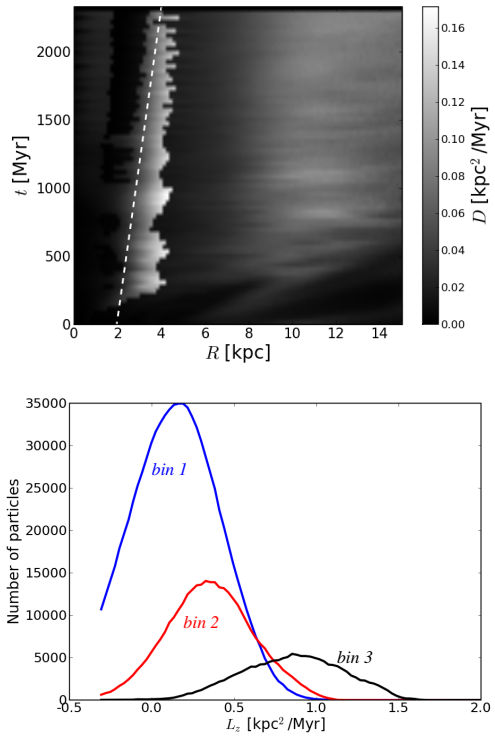


Figure 5 *Top:* Contour map of the diffusion coefficient D. *Bottom:* L_z-values of the particles at time 2.2 Gyr within the radial ranges $R = (2.5 \pm 0.5)$ kpc (bin 1, blue line), $R = (3.0 \pm 0.5)$ kpc (bin 2, red line) and $R = (8.0 \pm 0.5)$ kpc (bin 3, black line).

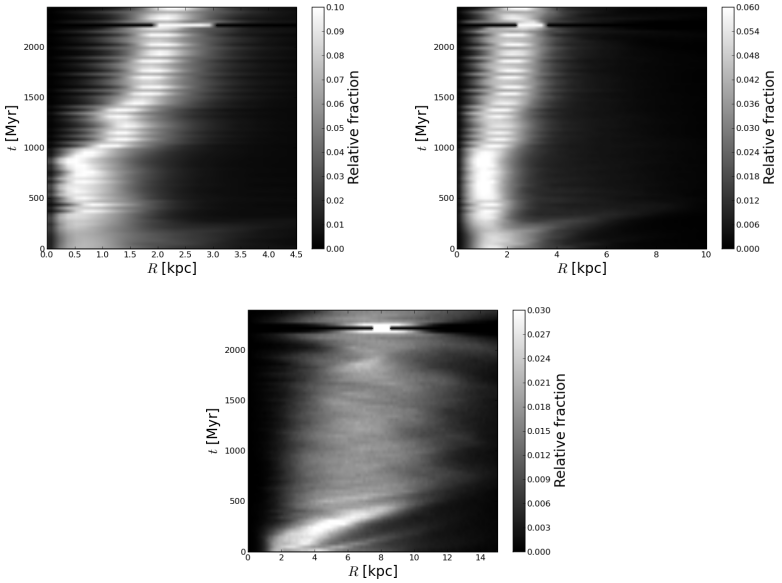


Figure 6 Radial migration of particles which at time $t = 2.2$ Gyr are in $R = (2.5\pm0.5)$ kpc (*left panel*), $R = (3.0 \pm 0.5)$ kpc (*middle panel*) and $R = (8.0 \pm 0.5)$ kpc (*right panel*).

volume of radius $d \sim 100$ pc around, for example, $R = 8$ kpc is very low for times less than the diffusion time, since $d \ll \sigma \sim 5$ kpc.

Three different bins of particles located respectively in $R = (2.5 \pm 0.5)$ kpc, $R = (3.0 \pm 0.5)$ kpc, $R = (8.0 \pm 0.5)$ kpc at $t = 2.2$ Gyr are followed in time and their evolution history is shown in Fig. 6. In the first bin, particles are inside the bar and they remain there all along the evolution. The presence of a $m = 1$ mode in the central bar region can be observed as periodical modulations in the density. These particles have values of $L_z \sim 0$ (see the bottom panel of Fig. 5, blue line labeled as 'bin 1') and large negative energies (see the left panel of Fig. 7). Particles in the second bin centered in $R = (3.0 \pm 0.5)$ kpc at $t = 2.2$ Gyr belong to two different types of orbits: one family can migrate only inside, the other can go outside the bar, in the disk. Large values of the diffusion coefficient D near the corotation region (see the top panel of Fig. 5) are related to this superposition of two families of bar orbits. The corresponding values of L_z and E are shown, respectively, in the red line in Fig. 5 (bottom panel, line labeled as 'bin 2') and in the middle panel of Fig. 7, where it can be easily seen that the two families have two different ranges of energies: large negative energies correspond to particles confined into the bar, while small negative energies correspond to particles which can span part of the disk. In the third bin, particles belong to the disk component: they can span all the region outside corotation, $R_c < R < 12$ kpc, and they come mainly from the corotation region at the time when the bar strength had a maximum (i.e. at $t \sim 350$ Myr, cf. the right panel of Fig. 1). These disk particles have small negative energies (see the right panel of Fig. 7) and large values of L_z (see the black line labeled as 'bin 3' in the bottom panel of Fig. 5).

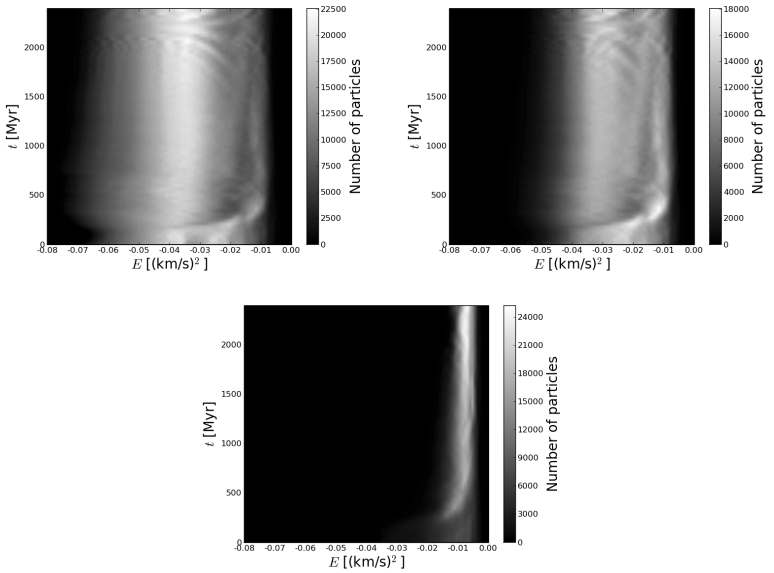


Figure 7 Energies of particles which at time $t = 2.2$ Gyr are in $R = (2.5 \pm 0.5)$ kpc (*left panel*), $R = (3.0 \pm 0.5)$ kpc (*middle panel*) and $R = (8.0 \pm 0.5)$ kpc (*right panel*).

5 Conclusions

Modeling the migration of stars in marginally stable disks as a diffusion process in the radial direction is a powerful tool which allows us to estimate quantitatively two crucial parameters, the diffusion coefficient and the diffusion time-scale. It is important to note that such diffusion model is only valid for describing the system for times smaller than the diffusion time-scale, which is of the order of the rotation period, and for times larger than the chaotic time-scale, after which orbits are no more time-reversible.

The calculations of both the diffusion coefficient and the diffusion time-scale give us a quantitative measure of the migration process in the disk. Another advantage of studying the diffusion of stars in real space, rather than in velocity space, is that it can be easily related to the evolution of chemical elements, thus representing an interesting tool to be implemented in chemical evolution codes.

We have found that the diffusion time-scale is of the order of one rotation period and that the diffusion coefficient D depends on the evolution history of the disk and on the radial position. Larger values D are found near the corotation region, which evolves in time, and in the external region, where asymmetric patterns develop. Marginally stable disks, with $Q_{\rm T} \sim 1$, have two different families of bar orbits with different values of angular momentum L_z and energy E, which determine a large diffusion in the corotation region.

The application of the method described here to models which include the halo component and have disks with different initial Safronov–Toomre parameter $Q_{\rm T}$ is presented in [35].

Acknowledgements

The simulations were run on the REGOR cluster at Geneva Observatory. This work has been supported by the Swiss National Science Foundation.

References

[1] Delgado-Serrano, R., Hammer, F., Yang, Y.B., & al. 2010, Astron. Astrophys., 509, A78
[2] Eskridge, P. B., Frogel, J. A., Pogge, R. W., et al. 2000, Astrophys. J., 119, 536–544
[3] Revaz, Y., & Pfenniger, D. 2004, Astron. Astrophys., 425, 67–76
[4] Bournaud, F., & Combes, F. 2002, Astron. Astrophys., 392, 83–102
[5] Binney, J., Dehnen, W., & Bertelli, G. 2000, Mon. Not. R. Astron. Soc., 318, 658-664
[6] Gerssen, J., Kuijken, K., & Merrifield, M.R. 2000, Mon. Not. R. Astron. Soc., 317, 545-549
[7] Shapiro, K.L., Gerssen, J., van der Marel, R.P. 2003, Astrophys. J., 126, 2707–2716
[8] Wielen, R. 1977, Astron. Astrophys., 60, 263–275
[9] Binney, J.J. & Tremaine, S. 2008, Galactic Dynamics: Second Edition (Princeton University Press), p. 693
[10] Spitzer, L. Jr., & Schwarzschild, M. 1951, Astrophys. J., 114, 385
[11] Spitzer, L. Jr., & Schwarzschild, M. 1953, Astrophys. J., 118, 106
[12] Lacey, C.G. 1984, Mon. Not. R. Astron. Soc., 208, 687–707
[13] Barbanis, B., & Woltjer, L. 1967, Astrophys. J., 150, 461
[14] Carlberg, R.G., & Sellwood, J.A. 1985, Astrophys. J., 292, 79–89
[15] Fuchs, B. 2001, Mon. Not. R. Astron. Soc., 325, 1637-1642
[16] Binney, J., & Lacey, C. 1988, Mon. Not. R. Astron. Soc., 230, 597–627
[17] Jenkins, A., & Binney, J. 1990, Mon. Not. R. Astron. Soc., 245, 305–317
[18] Edvardsson, B., Andersen, J., Gustafsson, B., et al. 1993, Astron. Astrophys., 275, 101
[19] Sellwood, J. A., & Binney, J. J. 2002, Mon. Not. R. Astron. Soc., 336, 785–796
[20] Minchev, I., & Famaey, B. 2010, Astrophys. J., 722, 112–121
[21] Minchev, I., Famaey, B., Combes, F., et al. 2011, Astron. Astrophys., 527, A147
[22] Grenon, M. 1972, in Cayrel de Strobel, G., & Delplace, A.M., eds., Proc. IAU Colloq. 17, Age des Etoiles, p. 55
[23] Castro, S., Rich, R.M., Grenon, M., et al. 1997, Astron. J., 114, 376–387
[24] Grenon, M. 1999, Astrophys. & Space Science, 265, 331–336
[25] Haywood, M. 2008, Mon. Not. R. Astron. Soc., 388, 1175–1184
[26] Lépine, J.R.D., Acharova, I.A., & Mishurov, Y. 2003, Astrophys. J., 589, 210–216
[27] Roškar, R., Debattista, V.P., Quinn, T.R., et al. 2008, Astrophys. J., 684, L79–L82
[28] van den Bergh, S. 1962, Astrophys. J., 67, 486–490
[29] Schmidt, M. 1963, Astrophys. J., 137, 758–769
[30] Pagel, B.E.J. 1997, Nucleosynthesis and chemical evolution of galaxies (Cambridge University Press)

[31] Chiappini, C., Matteucci, F., & Gratton, R. 1997, Astrophys. J., 477, 765–780
[32] Chiappini, C., Matteucci, F., & Romano, D. 2001, Astrophys. J., 554, 1044–1058
[33] Schönrich, R., & Binney, J.J. 2009, Mon. Not. R. Astron. Soc., 396, 203
[34] Schönrich, R., & Binney, J. J. 2009, Mon. Not. R. Astron. Soc., 399, 1145
[35] Brunetti, M., Chiappini, C., & Pfenniger, D. 2011, Astron. Astrophys., 534, A75
[36] Pfenniger, D., & Friedli, D. 1991, Astron. Astrophys., 252, 75–93
[37] Springel, V., Yoshida, N., & White, S. D. 2001, New Astron., 6, 79
[38] Springel, V. 2005, Mon. Not. R. Astron. Soc., 364, 1105–1134
[39] Sparke, L.S., & Sellwood, J.A. 1987, Mon. Not. R. Astron. Soc., 225, 653–675
[40] Fux, R. 1997, Astron. Astrophys., 327, 983–1003
[41] Gradsteyn, I.S., & Ryzhik, I.M. 2007, Table of integrals, series, and products, Jeffrey, A., & Zwillinger, D., eds., Seventh edition (Academic Press)